A computational study of trailing edge noise suppression with embedded structural compliance EP

iD Irsalan Arif, iD Randolph C. K. Leung and iD Muhammad Rehan Naseer

COLLECTIONS

EP This paper was selected as an Editor's Pick

A computational study of trailing edge noise suppression with embedded structural compliance

Irsalan Arif, [ID] Randolph C. K. Leung,[a) [ID] and Muhammad Rehan Naseer [ID]

Department of Mechanical Engineering, The Hong Kong Polytechnic University, Hong Kong, People's Republic of China

irsalan.arif@connect.polyu.hk, mmrleung@polyu.edu.hk, rehan.naseer@connect.polyu.hk

Abstract: A unique concept for suppression of trailing edge noise scattering from a splitter plate in a low Reynolds number flow is proposed. The key idea of the concept is the adoption of a structural compliance system embedded with a finite number of elastic panels. Specific compliance system designs are devised for promotion of panel structural resonance that effectively absorbs broadband flow/acoustic fluctuation energy responsible for noise scattering. The concept is examined using high-fidelity direct aeroacoustic simulation together with spatiotemporal aeroacoustic-structural interaction analysis. The concept is confirmed feasible and outperforms many similar trailing edge noise reduction approaches reported in the literature.
© 2023 Author(s). All article content, except where otherwise noted, is licensed under a Creative Commons Attribution (CC BY) license (http://creativecommons.org/licenses/by/4.0/).

1. Introduction

Trailing edge noise, the acoustic wave generated by the scattering of boundary layer instability off the sharp trailing edge of a rigid structure, is a fundamental source mechanism of fluid–structure interaction noise for aircraft, wind turbines, and air-moving devices (Brooks and Hodgson, 1981; Curle, 1955; Howe, 1984). It is widely recognized as one of the key factors that limits the operational capabilities and sustainable design of these engineering systems. Consequently, much work on new design ideas for trailing edge noise suppression has been carried out. Attempts have been made to replace part of the trailing edge with porous materials and achieve some noise reduction (Ali *et al.*, 2018; Kisil and Ayton, 2018). Bae *et al.* (2008) numerically investigated the aeroacoustics of a splitter plate with elastic cantilever end at a low Reynolds number and observed noise reduction as well as amplification at the cantilever natural frequency. The numerical study of Nardini *et al.* (2020) for a similar configuration involving external excitation showed some noise reduction/amplification depending on the relative amplitude and phase of the incident flow unsteadiness and edge structural motion. Jaworski and Peake (2013) and Cavalieri *et al.* (2016) combined these ideas to make the cantilever edge poroelastic, which was shown to be able to provide better noise reduction over a broader range of frequencies. Recently, Serrano-Galiano *et al.* (2018) and Kolb and Schaefer (2021) moved one step further to study the aeroacoustics of full membrane airfoil/plate. Their results indicate that a fully elastic structure can effectively delay the occurrence of stall, but it is ineffective in noise suppression and leads to noise amplification at certain flow conditions.

Although all the aforementioned ideas were able to reduce trailing edge noise to different extents, they are foreseen to have various limitations that make their applications in real-world noise control difficult. The use of porous materials certainly increases skin friction drag, not to mention the ease of losing its noise reduction due to the blockage of its pores by dirt or debris. In the cases with long flexible trailing edges or fully elastic plates, the overall structural integrity becomes questionable as these structures may experience aeroelastic divergence or flutter in designed flow conditions (Dowell, 1974). These undesirable side effects not only result in extra vibroacoustic sources for noise amplification but can also jeopardize the overall aerodynamic performance and safety of the engineering system as well.

In the present study, we propose a novel concept of trailing edge noise reduction without introducing side effects of increased drag, compromised structural integrity, or aeroelastic flutter. In short, we design a structural compliance system embedded with a finite number of elastic panels. Each panel is clamped at all edges. Unlike the ideas with a cantilever edge, the structural integrity of the original trailing edge can be preserved. In addition, the panel structural properties are carefully designed to make the fluid-loaded panel natural frequencies coincide with the intended range of frequency of noise reduction. Such settings allow the panels to set into structural resonance under incoming acoustic excitation. The sustained structural resonance acts to absorb the energy of incoming acoustic fluctuation and boundary layer instability before they undergo scattering at the sharp edge. A similar phenomenon was observed in previous studies of fluid–structure

---

a)Author to whom correspondence should be addressed.

interaction between an elastic airfoil and oncoming periodic convective vortical excitation (Leung and So, 2001; Luk et al., 2004). One must note that the proposed embedded compliance design would allow noise reduction over a broad range of frequencies of interest and the system frequency range can be easily tuned with varying panel structural designs. These features are considered an advantage over existing ideas in the literature. For the sake of simplicity in proving the feasibility of the proposed concept, only low Reynolds number mean flow past the splitter plate that gives laminar boundary layer is considered in this Letter. It is believed that the same reduction mechanism is applicable to cases with turbulent boundary layers at higher Reynolds numbers.

2. Physical problem

The physical setup of the problem under consideration follows problem 2 of Category 4 adopted in the Fourth Computational Aeroacoustics Workshop on Benchmark problems (Dahl, 2004), which is popular in many studies of trailing edge noise (Bae et al., 2008; Nardini et al., 2020). Consider a baseline compressible mixing layer flow formed by a semi-infinite thin rigid splitter plate with its trailing edge at the origin in two dimensions [Fig. 1(a)]. The flow above and below the splitter plate has a freestream Mach number $M = 0.2$ with a boundary layer displacement thickness δ^* and momentum thickness θ at the trailing edge. The Reynolds number based on θ is $Re_\theta = 530$ and the Prandtl number is $Pr = 0.7$. The thin splitter plate has a blunt end and a width $h = 0.105\delta^*$ (i.e., $h/\theta = 0.208$). This choice of plate width not only effectively avoids self-noise generation by edge bluntness which dominates whenever $h/\delta^* > 0.3$ (Brooks and Hodgson, 1981) but also supports sufficient mesh resolution for resolving the scattering at the edge. A weak broadband acoustic excitation is set upstream of the boundary layer over the upper plate surface to initiate scattering at plate trailing edge [Fig. 1(a)].

The proposed concept introduces embedded structural compliance, realized by replacement of multiple plate segments by elastic panels, to the splitter plate for achieving the suppression of noise scattering from plate trailing edge. The length of all elastic panels L is carefully chosen equal to 95θ for two reasons. First, it provides sufficient space for interaction between panel vibration and flow fluctuations, even in small scales comparable to plate boundary layer thickness. Second, it is shorter than the dominant wavelength of convective flow fluctuations of the baseline flow λ_{conv} ($\sim128\theta$) so that the flow-induced vibration of any short panel would not act as an additional acoustic source itself to radiate energy to far-field (Fahy and Gardonio, 2007). The necessity of the latter criterion was confirmed in a recent study of utilization of flow-induced vibrating panels for airfoil tonal noise suppression (Arif et al., 2020a). The conceptual compliance system is composed of three panels separated by $0.1\,L$ and is laid at a distance of $0.3\,L$ from the trailing edge [Fig. 1(b)]. The edges of each panel are rigidly clamped. In the present study, two compliance system designs are considered, one with its fluid-loaded panel resonant frequencies increasing along mean flow direction (CS1), and another decreasing along mean flow direction (CS2).

3. Numerical methodology

For the sake of convenience in analysis, all the variables are considered in their dimensionless forms taking freestream flow properties (velocity $\hat{U}_\infty$, density ρ_∞, and temperature T_∞) and panel length $\hat{L}$ as reference, where the symbols with hat (ˆ) denote their dimensional quantities. As such, the Reynolds number Re_L of the freestream is 5×10^4. In the present study, we adopt the direct aeroacoustics (DAS) approach for its capability of resolving the inherent coupling between the unsteady aerodynamic and acoustic solutions with high accuracy. The problem is modeled by compressible Navier–Stokes (N-S) equations and the equation of state which govern all relevant aeroacoustic behaviors. The two-dimensional N-S equations can be written in strong conservative form as

$$\frac{\partial \boldsymbol{U}}{\partial t} + \frac{\partial (\boldsymbol{F} - \boldsymbol{F}_v)}{\partial x} + \frac{\partial (\boldsymbol{G} - \boldsymbol{G}_v)}{\partial y} = 0, \tag{1}$$

where $\boldsymbol{U} = [\rho \ \ \rho u \ \ \rho v \ \ \rho E]^T$, $\boldsymbol{F} = [\rho u \ \ \rho u^2 + p \ \ \rho uv \ \ (\rho E + p)u]^T$, $\boldsymbol{F}_v = (1/Re)[0 \ \ \tau_{xx} \ \ \tau_{xy} \ \ \tau_{xx}u + \tau_{xy}v - q_x]^T$, $\boldsymbol{G} = [\rho v \ \ \rho uv \ \ \rho v^2 + p \ \ (\rho E + p)v]^T$, and $\boldsymbol{G}_v = (1/Re)[0 \ \ \tau_{xy} \ \ \tau_{yy} \ \ \tau_{xy}u + \tau_{yy}v - q_y]^T$ are the flow flux conservation variables, ρ is the density of
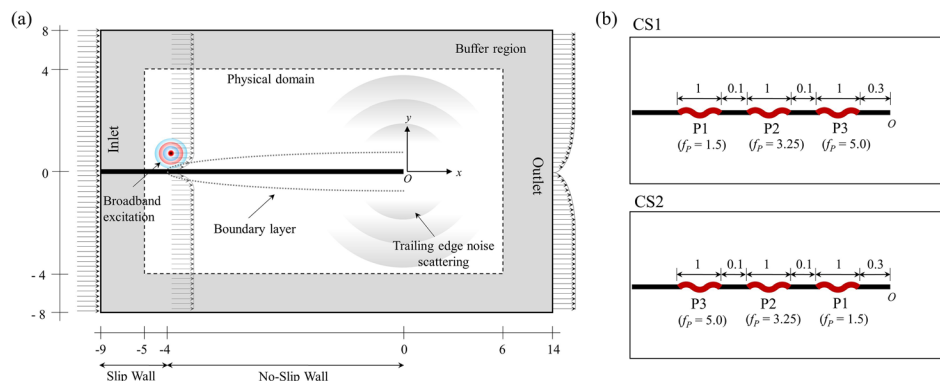

Fig. 1. (a) Schematic sketch of the computational domain (not to scale). (b) Panel arrangements for the compliance system designs.

fluid, u and v are the velocities in x and y direction, respectively, τ_{xx}, τ_{xy}, and τ_{yy} are the normal and shear stresses, and q_x and q_y are the heat fluxes. The total energy and pressure are calculated by $E = p/\rho(\gamma-1) + (u^2+v^2)/2, p = \rho T/\gamma M^2$. The non-dimensional time and frequency are defined by $t = \hat{t}\hat{U}_\infty/\hat{c}$ and $f = \hat{f}\hat{c}/\hat{U}_\infty$, respectively.

To solve the unsteady N-S equations, the conservation element and solution element (CE/SE) method is adopted. It is a robust and low-dissipative method that strictly enforces physical conservation laws in N-S equations in spatial and time domains. Details of its formulation and implementation are referred to Lam *et al.* (2014). The method has been successfully applied to analyze the complex aeroacoustic interactions at external and internal subsonic flow problems (Arif *et al.*, 2020b; Lam and Leung, 2018).

The computational domain is discretized into a structured mesh composed of 3400×1200 mesh elements. The mesh sizes around the plate trailing edge are carefully chosen to give minimum spacings of $\Delta x = 1.9 \times 10^{-4}$ and $\Delta y = 1.2 \times 10^{-4}$, respectively, so as to ensure there are at least 16 mesh elements across the plate thickness. The mesh is smoothly stretched in the x and y directions away from the plate to save computational cost. In the application of the CE/SE scheme, a quadrangle mesh element is split into four triangles using diagonal cross-divisions (Lam *et al.*, 2014). Hence, a total mesh size of 1.6×10^7 elements is generated to accurately resolve the flow fluctuations propagating in the proximity to the plate and acoustic propagation to the far-field. Combined sliding and no-slip boundary conditions are prescribed on all top and bottom plate surfaces. The changeover point between sliding and no-slip conditions on a surface is set to allow the naturally evolving boundary layer to give prescribed $Re_\theta = 530$ at plate edge. Except at the inlet, buffer zones with exponentially stretching meshes terminated with non-reflecting boundary condition are attached to all open physical domain boundaries as such treatment is effective in suppressing erroneous numerical waves propagating toward domain interior (Arif *et al.*, 2020a; Lam *et al.*, 2014). Time-marching of solution to Eq. (1) begins with the steady solution to the compressible boundary layer equations with zero pressure gradient on both sides of the splitter plate with a time step size $\Delta t = 1 \times 10^{-5}$ for a non-dimensional time episode of $t = 200$ and its time-stationary solution is taken as the baseline flow. A weak broadband excitation is introduced to the solution, which mainly serves to stimulate the natural flow instabilities within the laminar boundary layer, which are expected to scatter at the trailing edge of the flat plate to generate an acoustic wave (Nardini *et al.*, 2020). The excitation is modeled as a monopole at $(x,y) = (-3.9, 0.02)$ with fluctuating pressure defined as $p'_{inc} = p_A \sum_{k=1}^{72} \sin(2\pi t f_{exc,k} + \phi_k)$, where $p_A = 10^{-5}$. The excitation frequencies cover $1.5 \leq f_{exc,k} \leq 5$ with a uniform increment $\Delta f_{exc,k} = 0.05$ and random phases ϕ_k. The choice of the excitation frequency range comes with two reasons in mind. On the one hand, it allows at least one wavelength of scattered noise at the lowest excitation frequency to be captured in the physical domain, while, on the other hand, it provides sufficient resolution to the wavelength of the highest excitation frequency by the mesh. With these numerical settings, the acoustic wave amplitude produced by flow scattering is nearly 30 dB higher than pA and nearly 40 dB higher than the baseline flat plate self-noise (without excitation). As such, there is sufficient numerical room for capturing and exhibiting the effects of the compliance system in noise suppression.

The nonlinear dynamic response of an elastic panel is modeled by solving the one-dimensional plate equation to its simplest approximation (Dowell, 1974; Visbal and Gordnier, 2004). The governing equation for panel displacement, normalized by aforementioned flow reference variables, can be written as

$$S_P \frac{\partial^4 w}{\partial x^4} - (T_P + N_P)\frac{\partial^2 w}{\partial x^2} + \rho_P h_P \frac{\partial^2 w}{\partial t^2} + C_P \frac{\partial w}{\partial t} + K_P w = p_{ex}, \tag{2}$$

where w is the panel displacement from its undisturbed position, S_P is the panel bending stiffness, T_P is the external tensile stress in tangential direction, h_P is thickness of panel, N_P is the internal tensile stress in the tangential direction, C_P is the structural damping coefficient of the panel, K_P is the stiffness of the foundation supporting the panel, and p_{ex} is the net pressure acting across panel surfaces (Arif *et al.*, 2020b). The nonlinear coupling between aeroacoustic fluctuation and panel structural dynamics is resolved with a monolithic scheme (Fan *et al.*, 2018).

A key requirement of the proposed concept is that the panel structural properties (density, thickness, and external tension) must be chosen to give coincidence between panel natural frequencies under fluid loading and the frequencies of incident/scattered noise and flow fluctuations. The normalized frequency of the nth panel vibration mode can be estimated by Arif *et al.* (2020b) and Blevins and Plunkett (1980),

$$(f_P)_n = \frac{n}{2L_P}\sqrt{\frac{T_P}{\rho_P h_P}} \bigg/ \sqrt{1 + \frac{L_P}{\pi n \rho_P h_P}}, \tag{3}$$

where L_P is the length of panel. In the present study, the three elastic panels P1, P3, and P2 in Fig. 1(b) are set to give flow-induced structural resonance, respectively, at the lowest frequency $f = 1.5$, the highest frequency $f = 5.0$, and their arithmetic mean ($f = 3.25$) of the excitation. Details of panel properties are presented in Table 1.

4. Results and discussion

In every case attempted in the present study, the scattered solution is determined from subtracting the baseline flow from the solution to Eq. (1) with excitation turned on in a time-synchronized manner. Although not shown, the baseline solutions with elastic panels do not give appreciable difference from that of fully rigid splitter plate.

Table 1. Designed panel parameters.

Panel	Coverage (x-direction) CS1 / CS2	Material	Density ρ_P	Resonant frequency f_P	Resonant mode n
P1	-3.5 to -2.5 / -1.3 to -0.3	Stainless steel	6367.34	1.5	2
P2	-2.4 to -1.4 / -2.4 to -1.4	Carbon fiber	2212.24	3.25	3
P3	-1.3 to -0.3 / -3.5 to -2.5	Silicon rubber	833.45	5.0	3

Figure 2 compares the streamwise distributions of scattered pressure fluctuations captured on the upper surface of splitter plate. In essence, we put the temporal flow pressure fluctuations, captured at all locations along the plate surface, through fast Fourier transform (FFT) to obtain their spectral amplitudes, characteristic frequencies, as well as their streamwise distribution. The spectra for the figure are calculated over a duration of $t = 10$ with fine sampling frequency of 1×10^5. Figure 2(a) shows that the suppression of the scattered instabilities within the boundary layers by the flow-induced vibration of the panels is prominent over the entire excitation frequency range. A closer look at the solution at the selected resonant frequencies would give further insight into the actions of the compliance system panels (Table 1). One can see that a panel not only resonates to absorb the flow energy at its designed frequency but also absorbs energy at other frequencies [Figs. 2(b)–(d)]. The combined effects from all the panels facilitate the strong overall broadband flow instability suppression as illustrated in Fig. 2(a).

For CS1, at each designed panel frequency, a sharp reduction of boundary layer instability from rigid plate solution due to flow-induced panel resonance is evident. At $f = 1.5$, a sharp suppression of boundary layer instability prevails over panel P1 ($x = -3.5$ to -2.5) as shown in Fig. 2(b). Albeit weaker, its subsequent suppression by two downstream panels is observed over panel P2 ($x = -2.4$ to -1.4) at $f = 3.25$ and over panel P3 ($x = -1.3$ to -0.3) at $f = 5$ [Figs. 2(c) and 2(d)]. Hence, an effective overall suppression of flow scattering at the trailing edge is resulted for CS1. It is interesting to note that when the arrangement of panel installation is reversed (CS2), the overall suppression becomes less effective [Figs. 2(b)–(d)]. For scattering suppression effectiveness, CS1 gives a significant overall reduction in p' magnitude of $\sim$65% as compared to $\sim$52% for CS2 [Fig. 2(e)]. This might be attributed to differences in the extent of continuous reduction at panel resonant frequencies in two systems [Figs. 2(f)–(h)]. These observations reveal that an effective compliance system should be designed in such a manner that allows the first panel to exhibit structural resonance at the lowest excitation frequency of interest and then downstream of it the remaining panels with progressively increasing resonant frequencies are placed.

Figures 3(a) and 3(b), respectively, show the FFT spectra of displacements of panel centers with a sampling frequency of 1×10^5. For CS1, the dominance of the desired structural resonant modes is evident on all the panels (cf. Table 1) so the designed frequency coincidence of the compliance system is fully achieved. However, the design achievement is not satisfactory in CS2. The vibration of upstream panel P3 occurs mainly at $f = 3.5$ (instead of the designed $f = 5.0$), whereas the downstream panels P2 and P1 vibrate at $f = 4.0$ and 1.8 (instead of the designed $f = 3.25$ and $f = 1.5$), respectively. Such off-resonant panel responses are believed to be responsible for less effective boundary layer instability suppression for their weaker energy absorption capability than fully resonant vibration. This phenomenon has a stronger implication to noise suppression as seen in the forthcoming discussion.

The resonant and off-resonant behaviors observed may be further analyzed with spatiotemporal evolution of the panel displacements [Figs. 3(c) and 3(d)]. In every case, the time-stationary solution within a duration of $t = 3$ is captured
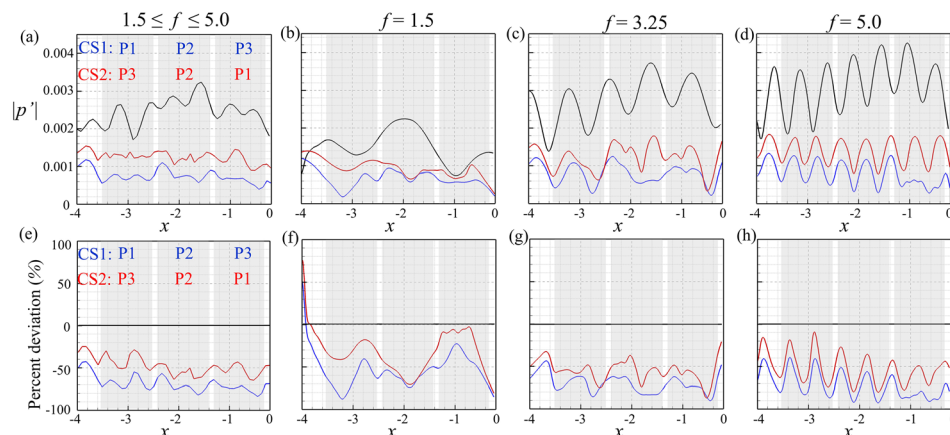

Fig. 2. (a)–(d) Streamwise distributions of scattered pressure fluctuation magnitudes on splitter plate upper surface. (e)–(h) Relative deviation in fluctuation amplitudes to the case of rigid plate. The shaded areas indicate the coverage of panels. ——, rigid plate; —— (blue), CS1; —— (red), CS2.
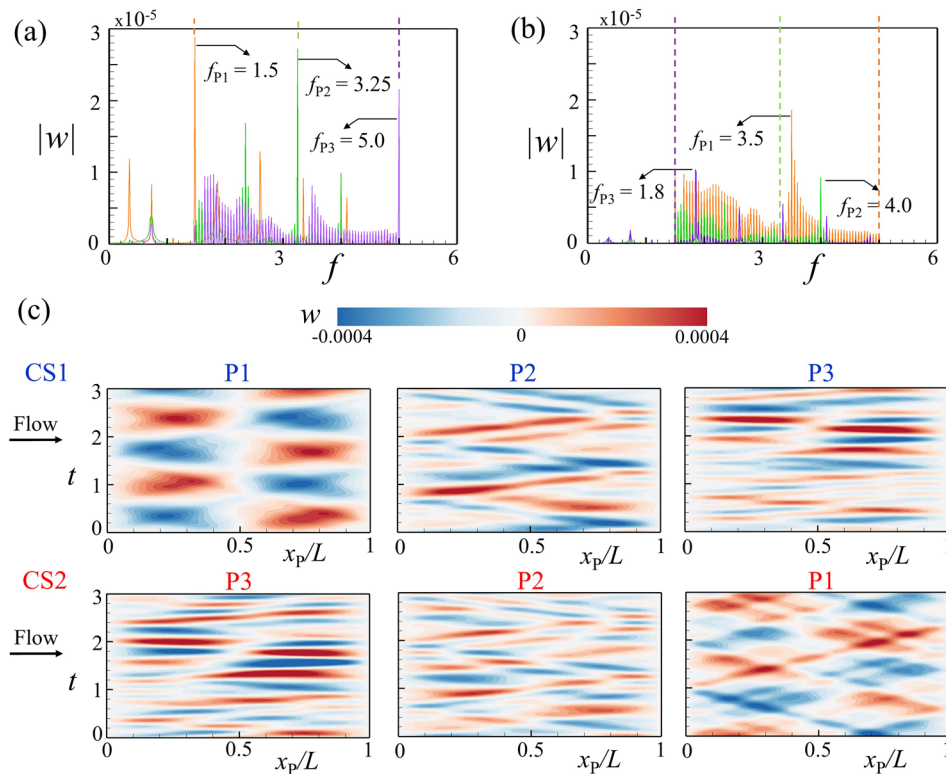
Fig. 3. Panel structural responses. (a) and (b), FFT spectra of panel centers of CS1 and CS2, respectively. (c) Spatio-temporal evolution of panel vibration. x_p, distance from panel leading edge. ——— (orange), P1; ——— (green), P2; ——— (red), P3.

in a time synchronized manner for analysis. The spatiotemporal variations of w of CS1 indicate that all panels can sustain their designed resonant modes around $w = 0$ and their corresponding standing waves on the panels are evident [Fig. 3(c)]. The panel P1 shows a more regular standing wave pattern than P2 and P3. This suggests a more coherent energy transfer from flow fluctuation prevails over the longer resonant wavelength of P1 for sustaining its vibration. The maximum panel displacements are found approximately two orders of the magnitude weaker than the local displacement thickness δ^* so the mean flow characteristics remain unaffected by panel dynamics. The panel responses of CS2 differ from CS1 [Fig. 3(d)]. The upstream panel is unable to vibrate in its designed resonant mode and neither are the two panels downstream. The upstream panel P3 vibrates with its maximum displacement comparable to boundary layer thickness. It may distort the mean flow characteristics which can adversely affect the flow-panel coupling of P2 and P1 downstream so their maximum displacements are at least one order of magnitude weaker than P3. The coherent energy transfer between flow and panel for P1 is thus impossible in CS2. As a result, no standing wave emerges in all CS2 panels. Each panel just carries two oppositely traveling bending waves bouncing between its two edges.

We now investigate the impact of the embedded compliance systems on the trailing edge noise scattering. In Figs. 4(a) and 4(b), the acoustic spectra captured right above and below the trailing edge clearly show the suppression of trailing edge noise scattering. A fairly uniform 10 dB reduction over the entire frequency range of interest is observed for CS1. However, CS2 gives much lower reduction at low to mid frequencies which leads to much lower overall reduction. All these observations support the fact that the flow instability energy is effectively absorbed by the compliance systems before the scattering occurs at the trailing edge of splitter plate.

The extent of noise suppression can be ascertained by the azimuth distribution of sound pressure level reduction ($\Delta SPL_{\text{reduction}} = -20 \times \log_{10}(p'_{\text{rms,CS}}/p'_{\text{rms,rigid}})$) at a radius $r = 3$ from the plate trailing edge. The radial axis in the plot corresponds to frequency ranging from $f = 0$–5. The $\Delta SPL_{\text{reduction}}$ for both systems [Figs. 4(c) and 4(d)] show a much higher overall noise reduction above the splitter plate than below. For both systems, maximum noise reduction is obtained within the sector $60° \leq \theta \leq 120°$. For CS1, the $\Delta SPL_{\text{reduction}}$ remains fairly constant up until $f = 1.5$ in all azimuthal locations above the splitter plate. However, for $f > 1.5$, its constancy is lost and shows a pattern skewed towards upstream direction. It is interesting to see a similar skewed $\Delta SPL_{\text{reduction}}$ pattern prevails below the plate even the broadband excitation is activated above the plate. For CS2, a similar azimuthal distribution prevails but with weaker $\Delta SPL_{\text{reduction}}$. In fact, its skewing starts at a much lower frequency (i.e., $f = 1.5$) than CS1. This might be attributed to the fact that the upstream panel P3 (designed with the highest resonant frequency) does not provide sufficient suppression to flow instability at low frequencies. Table 2 shows a comparison of the noise reduction performance of the proposed concept with results reported in existing literature.
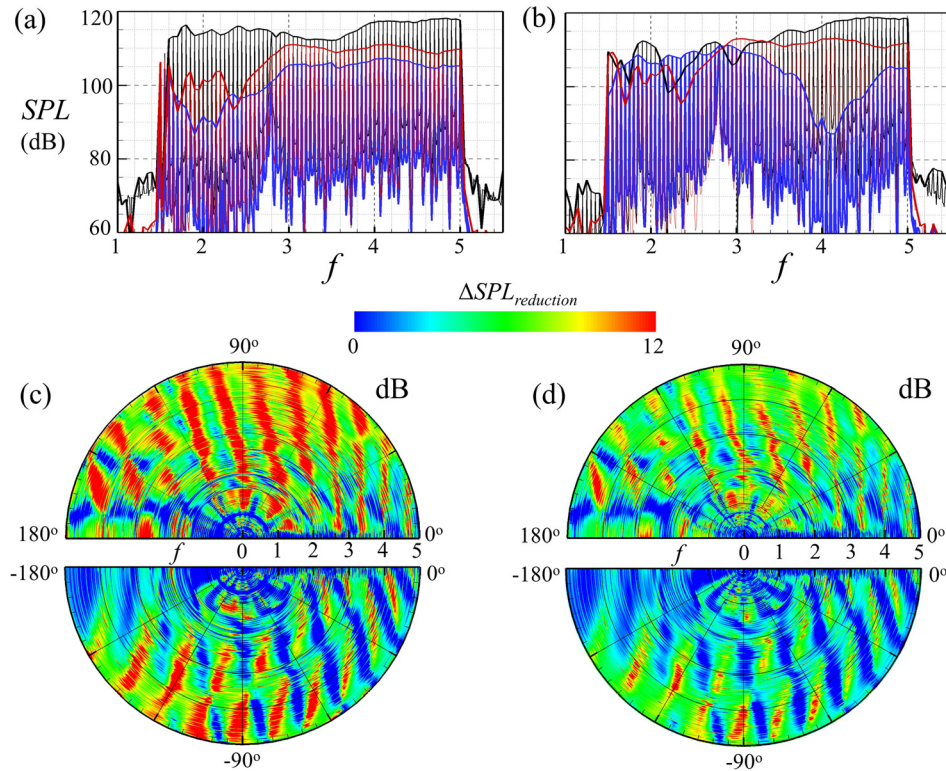
Fig. 4. (a) and (b), Acoustic pressure spectra captured at $(x, y) = (0, 3)$ and $(x, y) = (0, -3)$, respectively. (c) and (d), Azimuthal distribution of $\Delta SPL_{\text{reduction}}$ of CS1 and CS2, respectively. ——, rigid plate; —— (blue), CS1; —— (red), CS2.

The superior performance of the proposed concept is observed in the present study. It is interesting to note that both of the compliance systems provide the highest azimuthally averaged (Avg) $\Delta SPL_{\text{reduction}}$ among those listed. This shows clearly the high effectiveness of the proposed systems in suppressing the trailing edge noise scattering capability.

5. Conclusions

In this Letter, we propose a unique concept for broadband suppression of noise produced by the scattering at the trailing edge of a semi-infinite thin splitter plate in a low Reynolds number flow. In essence, the idea comprises a structural compliance system embedded with three rigidly clamped elastic panels. The compliance system facilitates absorption of incident flow fluctuation energy responsible for scattering by means of panel structural resonance arising from the coincidence between their fluid-loaded panel natural frequencies with a frequency range of noise reduction of interest. The feasibility of the concept is studied using high-fidelity direct aeroacoustic simulation with two compliance system designs accompanied with spatiotemporal aeroacoustic–structural interaction analysis. The numerical results clearly elucidate the

Table 2. Comparison with existing ideas for trailing edge noise suppression. A, analytical study; E, experimental study; N, numerical study, TE trailing edge.

Idea	M	Re	Study	Avg $\Delta SPL_{\text{reduction (dB)}}$	Max $\Delta SPL_{\text{reduction (dB)}}$	Max $\Delta SPL_{\text{amplification (dB)}}$
Cantilevered elastic TE (Nardini et al., 2020)	0.4	7.5×10^4	N	7.5	10	—
Cantilevered elastic TE (Bae et al., 2008)	0.4	4.4×10^4	N	2.5	20	15
Porous TE (Kisil and Ayton, 2018)	0.6	—	A	1.0	2.4	0.1
Porous TE (Ali et al., 2018)	0.076	1.6×10^5	E	—	8.0	—
Poroelastic TE (Jaworski and Peake, 2013)	0.1	—	N	1.1	2.0	—
Poroelastic TE (Ayton, 2016)	0.01	—	A	4.2	10	0.5
Rigid serrated TE (Moreau and Doolan, 2013)	0.12	1.6×10^5	E	3	13	—
Embedded compliance system (Present study)	0.2	5.0×10^4	N	11.4 (CS1)	14.2 (CS1)	—
				8.7 (CS2)	10.3 (CS2)	—

fluid–structure interactions of two designs responsible for trailing edge noise suppression. Their superior noise suppression effectiveness to that of similar ideas in the literature is confirmed. As such, the feasibility of the proposed concept is firmly established. Given the high noise suppression and foreseen advantages in real-world realization of the proposed concept, it is envisaged that the outcomes reported would foster further analytical and experimental studies in short future.

References and links

Ali, S. A. S., Azarpeyvand, M., and Da Silva, C. R. I. (**2018**). "Trailing-edge flow and noise control using porous treatments," J. Fluid Mech. **850**, 83–119.

Arif, I., Lam, G. C. Y., Wu, D., and Leung, R. C. K. (**2020a**). "Passive airfoil tonal noise reduction by localized flow-induced vibration of an elastic panel," Aerosp. Sci. Technol. **107**, 106319.

Arif, I., Wu, D., Lam, G. C. Y., and Leung, R. C. K. (**2020b**). "Exploring airfoil tonal noise reduction with elastic panel using perturbation evolution method," AIAA J. **58**(11), 4958–4968.

Ayton, L. J. (**2016**). "Acoustic scattering by a finite rigid plate with a poroelastic extension," J. Fluid Mech. **791**, 414–438.

Bae, Y., Jang, J. Y., and Moon, Y. J. (**2008**). "Effects of fluid-structure interaction on trailing-edge noise," J. Mech. Sci. Technol. **22**(7), 1426–1435.

Blevins, R. D., and Plunkett, R. (**1980**). "Formulas for natural frequency and mode shape," J. Appl. Mech. **47**(2), 461–462.

Brooks, T. F., and Hodgson, T. (**1981**). "Trailing edge noise prediction from measured surface pressures," J. Sound Vib. **78**(1), 69–117.

Cavalieri, A., Wolf, W., and Jaworski, J. (**2016**). "Numerical solution of acoustic scattering by finite perforated elastic plates," Proc. R. Soc. A: Math. Phys. Eng. Sci. **472**(2188), 20150767.

Curle, N. (**1955**). "The influence of solid boundaries upon aerodynamic sound," Proc. R. Soc. London, Ser. A: Math. Phys. Sci. **231**(1187), 505–514.

Dahl, M. D. (**2004**). "Fourth computational aeroacoustics (caa) workshop on benchmark problems," in *Fourth Computational Aeroacoustics (CAA) Workshop on Benchmark Problems*, Ohio (September 2004), NASA/CP–2004-212954, pp. 25–26.

Dowell, E. H. (**1974**). "Linear theoretical aeroelastic models," in *Aeroelasticity of Plates and Shells* (Springer Science & Business Media, Springer, Dordrect, Germany), Vol. 1, pp. 35–38.

Fahy, F. J., and Gardonio, P. (**2007**). *Sound and Structural Vibration: Radiation, Transmission and Response* (Jordan Hill, Oxford, UK).

Fan, H. K. H., Leung, R. C. K., Lam, G. C. Y., Aurégan, Y., and Dai, X. (**2018**). "Numerical coupling strategy for resolving in-duct elastic panel aeroacoustic/structural interaction," AIAA J. **56**(12), 5033–5040.

Howe, M. (**1984**). "On the generation of sound by turbulent boundary layer flow over a rough wall," Proc. R. Soc. London, A: Math. Phys. Sci. **395**(1809), 247–263.

Jaworski, J. W., and Peake, N. (**2013**). "Aerodynamic noise from a poroelastic edge with implications for the silent flight of owls," J. Fluid Mech. **723**, 456–479.

Kisil, A., and Ayton, L. J. (**2018**). "Aerodynamic noise from rigid trailing edges with finite porous extensions," J. Fluid Mech. **836**, 117–144.

Kolb, E., and Schaefer, M. (**2021**). "Aeroacoustic simulation of flexible structures in low mach number turbulent flows," Comput. Fluids **227**, 105020.

Lam, G. C. Y., and Leung, R. C. K. (**2018**). "Aeroacoustics of NACA 0018 airfoil with a cavity," AIAA J. **56**(12), 4775–4786.

Lam, G. C. Y., Leung, R. C. K., Seid, K. H., and Tang, S. K. (**2014**). "Validation of CE/SE scheme in low mach number direct aeroacoustic simulation," Int. J. Nonlinear Sci. Numer. Simul. **15**(2), 157–169.

Leung, R. C. K., and So, R. M. C. (**2001**). "Noise generation of blade–vortex resonance," J. Sound Vib. **245**(2), 217–237.

Luk, K. F., So, R. M. C., Leung, R. C. K., Lau, Y. L., and Kot, S. C. (**2004**). "Aerodynamic and structural resonance of an elastic airfoil due to oncoming vortices," AIAA J. **42**(5), 899–907.

Moreau, D. J., and Doolan, C. J. (**2013**). "Noise-reduction mechanism of a flat-plate serrated trailing edge," AIAA J. **51**(10), 2513–2522.

Nardini, M., Sandberg, R. D., and Schlanderer, S. C. (**2020**). "Computational study of the effect of structural compliance on the noise radiated from an elastic trailing-edge," J. Sound Vib. **485**, 115533.

Serrano-Galiano, S., Sandham, N. D., and Sandberg, R. D. (**2018**). "Fluid–structure coupling mechanism and its aerodynamic effect on membrane aerofoils," J. Fluid Mech. **848**, 1127–1156.

Visbal, M., and Gordnier, R. (**2004**). "Numerical simulation of the interaction of a transitional boundary layer with a 2-D flexible panel in the subsonic regime," J. Fluids Struct. **19**(7), 881–903.